An applied variational framework integrating distortion correction, segmentation and cortical parcellation of diffusion MRI data

Oscar Esteban*, *Member, IEEE,* Alessandro Daducci, *Member, IEEE,* Meritxell Bach-Cuadra, *Member, IEEE,* Jean-Philippe Thiran, *Member, IEEE,* Andrés Santos, *Member, IEEE,* and Dominique Zosso, *Life Fellow, IEEE*

***Abstract*—In whole-brain connectivity analysis of diffusion MRI (dMRI) data, an accurate delineation of the white-matter and grey-matter interfaces is required. While high-standard segmentation is readily available for structural MRI, dMRI typically present significant cerebrospinal fluid contamination effects, mainly derived from its typical low resolution, and severe geometrical distortions. We propose a segmentation-registration variational framework that exploits the detailed anatomy extracted from structural MRI as shape-prior. We use an "active contours without edges"-like model to search for a deformation field that optimally maps the shape prior on multivariate dMRI-derived data in diffusion space, registering structural and diffusion coordinate spaces and implicitly segmenting dMRI data. The approach proven the intrinsic coupling of segmentation and distortion correction and we evaluate its results on a digital simulated phantom and real datasets. Therefore, precise and consistent cortical parcellation on dMRI is straightforward by projection from T1 space, avoiding additional registration, segmentation and/or surface matching steps.**

***Index Terms*—diffusion MRI, susceptibility distortion, segmentation, registration, parcellation, shape-prior.**

I. Introduction

DIFFUSION MRI (dMRI) is a widely used family of magnetic resonance (MR) techniques [1] which recently has accounted for a growing interest in its application to whole-brain structural connectivity analysis. This emerging field [2, 3], currently includes a large amount of imaging techniques for acquisition, processing, and analysis specifically tuned for diffusion MRI (dMRI) data [4].

The whole-brain connectivity analysis has given rise to some challenges towards reliable structural information about the neuronal tracts from dMRI [5, 6]. Here, we shall address brain tissue segmentation on diffusion space and correction of geometrical distortions inherent to the acquisition sequence [7].

In this work, we will refer as brain tissue segmentation to the precise delineation of the cerebrospinal fluid (CSF)-grey matter (GM) and GM-white matter (WM) interface surfaces. An accurate brain tissue segmentation is required to filter the fiber bundles obtained with dMRI tractography. This requirement is usually solved in practice by plainly thresholding the fractional anisotropy (FA), a well-known scalar map derived from dMRI which depicts the isotropy of water diffusion inside the brain. Also, it is necessary to locate the intersections of fiber bundles and GM. Moreover, a precise location of the GM-WM surface is also essential to finally achieve a consistent parcellisation of the cortex to represent the nodes of the output network. This parcellisation is generally defined in a high-resolution and better understood structural magnetic resonance imaging (MRI) of the same subject (e.g. T1-weighted (T1) and/or T2-weighted (T2) weighted acquisitions). Even though some efforts have addressed the study of the robustness of tractography with respect to intra-subject variability [8, 9], these results are restricted to certain regions of the brain, only. Therefore, robust and precise segmentation methods are required in the whole-brain application. The problem is challenging due to the much lower resolution of dMRI (typically around $2.0 \times 2.0 \times 2.0 mm^3$) compared to structural MRI, and the existence of geometrical distortions.

dMRI data are usually acquired with echo-planar imaging (EPI) sequences as they allow for very fast acquisitions, but they are known to suffer from geometrical distortions due to local field inhomogeneities. These artifacts happen along the phase-encoding direction, and are most appreciable in the front part of the brain for the strong air/tissue interface around the frontal sinuses. A number of methodologies have been developed to correct for the distortion, and are generically named as *EPI-unwarp* techniques [10, 11, 12, 13]. These methods usually require the extra acquisition of the magnitude and phase of the field ("field-mapping"), a condition which is not always met. Some other methodologies do not make use

Manuscript received XXX XX, 2013; revised XXX XX, 2013. This study is supported by: the Spain's Ministry of Science and Innovation (projects TEC2010-21619- C04-03, TEC2011-28972-C02-02, CDTI-CENIT AMIT and INNPACTO PRECISION), Comunidad de Madrid (ARTEMIS) and European Regional Development Funds; the Center for Biomedical Imaging (CIBM) of the Geneva and Lausanne Universities and the EPFL, as well as the Leenaards and Louis Jeantet foundations. *Asterisk indicates corresponding author*.

*O. Esteban is with the Biomedical Image Technologies (BIT), ETSI Telecomunicación, Universidad Politécnica de Madrid and CIBER-BBN, Madrid, Spain, and the Signal Processing Laboratory (LTS5), École Polytechnique Fédérale de Lausanne (EPFL), Lausanne, Switzerland (e-mail: phd@oscaresteban.es).

A. Daducci is with the Signal Processing Laboratory (LTS5), École Polytechnique Fédérale de Lausanne (EPFL), Lausanne, Switzerland.

M. Bach-Cuadra and JP. Thiran are with the Signal Processing Laboratory (LTS5), École Polytechnique Fédérale de Lausanne (EPFL), Lausanne, Switzerland, and Dept. of Radiology, University Hospital Center (CHUV) and University of Lausanne (UNIL), Lausanne, Switzerland.

A. Santos is with the Biomedical Image Technologies (BIT), ETSI Telecomunicación, Universidad Politécnica de Madrid and CIBER-BBN, Madrid, Spain.

D. Zosso is with the Department of Mathematics, University of California, Los Angeles (UCLA), Los Angeles, CA, US and is supported by the Swiss National Science Foundation (SNF) under grant PBELP2-137727.

of the field-mapping, compensating the distortion with non-linear registration from structural MRI or other means [14]. To our knowledge, there exists no study on the impact of the EPI distortion on the variability of tractography results.

Therefore, the problems of precise segmentation in dMRI-space and the spatial mapping between these contours and the corresponding surfaces in anatomical images bear significant redundancy. Once the spatial relationship between T1 and dMRI space is established, the contours which are readily available in T1 space can simply be projected on to the dMRI-data. Conversely, if a precise delineation in dMRI-space was achieved, the spatial mapping with T1-space could be derived from one-to-one correspondences on the contours. However, neither segmentation nor registration can be performed flawlessly, if considered independently. The significant benefits of exploiting the anatomical MRI when segmenting the dMRI data have been demonstrated [15], justifying the use of the shape prior information.

We suggest clustering the current methodologies of template-based segmentation methods into three groups. The first group typically adds a shape prior term to the energy functional of an evolving active contour [**? ? ? ? ? ? ? ?**]. These methods generally have a explicit description of the expected relative boundary locations of the object to be delineated, and some even model the statistical deviations from this average shape. Closely related to this group are atlas-based segmentation methods [**? ? ? ? ?**], where the prior imposes consistent voxel-based classification of contiguous regions. Here, the presence of more structures than one unique region of interest (ROI) helps aligning the target image with the atlas in a hierarchical fashion. Finally, the third group generalizes the atlas to actual images, and the contour is to segment simultaneously two different target images, related by a spatial transform to be co-estimated [**? ?**].

In this paper we propose a novel registration framework to simultaneously solving the segmentation and distortion challenges, by exploiting as strong shape-prior the detailed morphology extracted from high-resolution anatomical MRI. Indeed, hereafter we assume this segmentation problem in anatomical images as a solved by widely used available procedures. Moreover, the shape prior is of very "strong" nature, since it is specific to the particular subject. Also, after global alignment using existing approaches, the remaining spatial deformation between anatomical and diffusion space is due to EPI distortions. Finally, we need to establish precise spatial correspondence between the surfaces in both spaces, including the tangential direction for parcellation. Therefore, we can reduce the problem to finding the differences of spatial distortion in between anatomical and diffusion weighted (DW) space. We thus reformulate the segmentation problem as an inverse problem, where we seek for an underlying deformation field (the distortion) mapping from the structural space into the diffusion space, such that the structural contours segment optimally the dMRI data. In the process, the one-to-one correspondence between the contours in both spaces is guaranteed, and projection of parcellisation to DW space is implicit and consistent.

We test our proposed joint segmentation-registration model on two different synthetic examples. The first example is a scalar sulcus model, where the CSF-GM boundary particularly suffers from partial volume effect (PVE) and can only be segmented correctly thanks to the shape prior and its coupling with the inner, GM-WM boundary through the imposed deformation field regularity. The second case deals with more realistic dMRI data stemming from phantom simulations of a simplistic brain data. Again, we show that the proposed model successfully segments the dMRI data based on two derived scalar features, namely FA and mean diffusivity (MD), while establishing an estimate of the dense distortion field.

The rest of this paper is organized as follows. First, in section II we introduce our proposed model for joint multivariate segmentation-registration. Then we provide a more detailed description of the data and experimental setup in section III. We present results in section IV and conclude in section V.

II. Methods

A. Active contours without edges based segmentation model

Let us denote $\{c_i\}_{i=1..N_c}$ the nodes of a shape prior surface. In our application, a precise WM-GM interface extracted from a high-resolution reference volume. All the formulations can be naturally extended to include more shape priors. On the other hand, we have a number of dMRI-derived features at each voxel of the volume. Let us denote by x the voxel and $f(x) = [f_1, f_2, \ldots, f_N]^T(x)$ its associated feature vector.
The transformation from reference into dMRI coordinate space is achieved through a dense deformation field $u(x)$, such that:

$$c_i' = T\{c_i\} = c_i + u(c_i) \tag{1}$$

Since the nodes of the anatomical surfaces might lay off-grid, it is required to derive $u(x)$ from a discrete set of parameters $\{u_k\}_{k=1..K}$. Densification is achieved through a set of associated basis functions Ψ_k (e.g. rbf, interpolation splines):

$$u(x) = \sum_k \Psi_k(x) u_k \tag{2}$$

Consequently, the transformation writes

$$c_i' = T\{c_i\} = c_i + u(c_i) = c_i + \sum_k \Psi_k(c_i) u_k \tag{3}$$

Based on the current estimate of the distortion u, we can compute "expected samples" within the shape prior projected into the dMRI. Thus, we now estimate region descriptors of the dMRI features $f(x)$ of the regions defined by the priors in dMRI space. Using Gaussian distributions as region descriptors, we propose an active contours without edges (ACWE)-like, piece-wise constant, variational image segmentation model (where the unknown is the deformation field) [16]:

$$E(u) = \sum_{\forall R} \int_{\Omega_R} (f - \mu_R)^T \Sigma_R^{-1} (f - \mu_R) dx \tag{4}$$

where R indexes the existing regions and the integral domains depend on the deformation field u. Note that minimizing this energy, $\mathrm{argmin}_u\{E\}$, yields the maximum a posteriori (MAP) estimate of a piece-wise smooth image model affected

by Gaussian additive noise. This inverse problem is ill-posed [17, 18]. In order to account for deformation field regularity and to render the problem well-posed, we include limiting and regularization terms into the energy functional [19, 20]:

$$E(u) = \sum_{\forall R} \{ \int_{\Omega_R} (f-\mu_R)^T \Sigma_R^{-1} (f-\mu_R) dx \} + \alpha \int \|u\|^2 dx + \beta \int \left(\|\nabla u_x\|^2 + \|\nabla u_y\|^2 + \|\nabla u_z\|^2 \right) dx \quad (5)$$

These regularity terms ensure that the segmenting contours in dMRI space are still close to their native shape. The model easily allows to incorporate inhomogeneous and anisotropic regularization [21] to better regularize the EPI distortion.

At each iteration, we update the distortion along the steepest energy descent. This gradient descent step can be efficiently tackled by discretizing the time in a forward Euler scheme, and making the right hand side semi-implicit in the regularization terms:

$$\frac{u^{t+1}-u^t}{\tau} = -\sum_{i=1}^{N_c} \left[e(f(c_i'))\hat{n}_{c_i'} \Psi_{c_i}(x) \right] - \alpha u^{t+1} + \beta \Delta u^{t+1} \quad (6)$$

where the data terms remain functions of the current estimate u^t, thus $c_i' = c_i'(u^t)$. For simplicity on notation, we restricted the number of priors to only 1. We also defined $e(f(c_i')) = E_{out}(f(c_i')) - E_{in}(f(c_i'))$, and $E_R(f) = (f-\mu_R)^T \Sigma_R^{-1} (f-\mu_R)$. We applied a spectral approach to solve this implicit scheme:

$$u^{t+1} = \mathcal{F}^{-1} \left\{ \frac{\mathcal{F}\{u^t/\tau - \sum_{i=1}^{N_c} \left[e(f(c_i'))\hat{n}_{c_i'} \Psi_{c_i}(x) \right] \}}{\mathcal{F}\{(1/\tau + \alpha)\mathcal{I} - \beta\Delta\}} \right\} \quad (7)$$

III. Data and Experiments

A. Shape prior

As described in section I, the general situation in the connectivity pipelines consists of having a reliable segmentation obtained from the high resolution T1 reference image. Therefore, a precise location of the tissue interfaces of interest is available in a reference space. Given that the anatomical reference segmentation is beyond the scope of this manuscript, we simply rely on the true contours known from the underlying models, and do not seek to establish them in a separate segmentation step on "anatomical" images.

B. Synthetic gray-scale data

The first simplified model to test the approach is inspired by a problem shown for coupled CSF/GM and GM/WM segmentation in [22]. Authors note that "partial volume effects blur the distinction between closely adjacent surfaces in deep sulci, leading to a well-known segmentation error in which the deeper reaches of sulci are not penetrated by the putative surface model." This problem is aggravated in DWI, since the resolution tends to be worse compared to the anatomical images considered in [22]. They test their coupled segmentation algorithm on an image, "representing a sulcus in which the distinction between opposing banks of the sulcus has been obscured by partial volume."

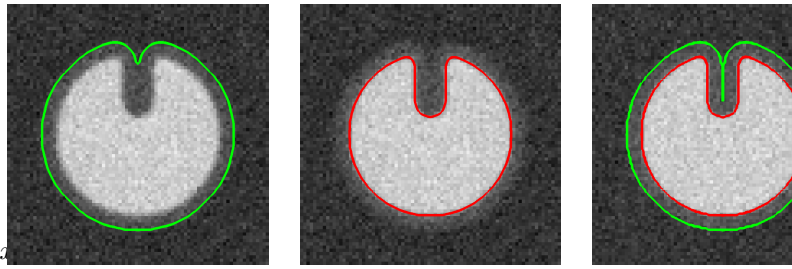

a) b) c)

Fig. 1. The gray-scale sulcus model. a) The apparent CSF/GM boundary is affected by partial volume in the sulcal cavity, and conventional segmentation is likely to miss it. b) The GM/WM interface here has consistently good contrast. c) Registering the two shape priors coupled through deformation field regularity is expected to guide the CSF/GM contour. d&e) 3D view of the two shape priors.

Here, we reproduce their model on a volume consisting of three piecewise-constant parts: a notched ball representing the WM with a single sulcus ($\mu_{WM} = 0.8$), a cortical sheet of GM obtained through dilation of the WM ($\mu_{GM} = 0.5$), and the surrounding background representing CSF ($\mu_{CSF} = 0.2$). The volume is then affected by additive Gaussian noise, effectively creating uniform standard deviation of $\sigma = 0.045$ per region.

As illustrated in Figure 1, conventional single surface segmentation of the CSF/GM boundary misses to capture the sulcus in its full depth. With our proposed model, we expect the joint segmentation-registration to be driven largely by the inner, GM/WM contour that exhibits sufficient contrast and lesser partial volume effects. The shape prior of the outer, difficult contour will then be co-aligned through the regularity of the estimated deformation field.

C. Simulated diffusion data

In order to demonstrate the functionality of the methodology, and characterize its possibilities with diffusion data, we built a synthetic phantom from a model consisting of several spherical shapes emulating the different brain tissues (see **??**, first row). We simulated a single-shell acquisition at $b = 1000$ (8) with 30 samples equally distributed on one hemisphere, corresponding to a standard diffusion tensor imaging (DTI) acquisition commonly used in clinical practice. We generated a synthetic displacement field to produce an EPI-like distortion on the dMRI signal. Finally, we reconstructed the deformed signal, and generated dMRI-derived scalar maps (specifically the FA and MD maps). Then, the scalar maps were placed as features in (5) to drive our segmentation approach, finding the location of the WM-GM and the CSF-WM interfaces in the distorted space.

a) Signal simulation: To numerically simulate the MRI signal attenuation when applying a diffusion gradient in a voxel with N fiber populations we made use of the standard

Multi-Tensor Model [**?**]:

$$S(q)/S_0 = \sum_{i=1}^{N} f_i \exp\left(-b\, q^T \mathbf{D}_i\, q\right) + f_{iso} \exp\left(-b\, \mathbf{D}_{iso}\right) + f_{gm} \exp\left(-b\, \mathbf{D}_{gm}\right) \quad (8)$$

where $q \in \mathbb{S}^2$ is the direction of the diffusion gradient applied, b is the b-value accounting for its strength and $S_0 \equiv S(0)$ is the signal with no diffusion weighting. f_i and $\mathbf{D}_i$ are the volume fraction and the diffusion tensor characterizing the i-th fiber population, whereas the tensors $\mathbf{D}_{iso}$ and $\mathbf{D}_{gm}$ describe the diffusion processes of partial volumes with CSF and GM within the voxel, which volume fractions are, respectively, f_{iso} and f_{gm}, and $\sum_i f_i + f_{iso} + f_{gm} = 1$. In this work, the diffusion properties have been taken from standard ranges typically observed in the human brain [**?**]. Moreover we assumed $N = 1$ and $S_0 = 1$ without loss of generality.

b) Noise simulation: The diffusion MRI signal S has been corrupted with *Rician noise* [**?**] as follows:

$$\tilde{S} = \sqrt{(S + \varepsilon_1)^2 + \varepsilon_2^2} \quad (9)$$

where $\varepsilon_{1,2}$ are Gaussian distributed with zero mean and standard deviation $\sigma = S_0/SNR$ and signal-to-noise ratio (SNR) is the SNR on the S_0 image.

c) Simulated EPI distortion: For this model, we created manually a sound distortion to approximate the real EPI distortions. We interpolated the distortion to a dense deformation field, and applied it to generate the deformed dMRI signal.

d) Derived scalar features: We obtained the local fiber configuration in each voxel with a commonly used DTI reconstruction tool [1]. The properties of the reconstructed tensors and derived scalar maps have been studied by [23]. Based on their findings, FA (10) and MD (11) are considered complementary features, and therefore we selected them for the energy model (5) in driving the registration-segmentation process. Whereas FA informs mainly about the *shape* of diffusion, the MD is more related to the *magnitude* of the process:

$$\mathrm{FA} = \sqrt{\frac{1}{2}} \frac{\sqrt{(\lambda_1 - \lambda_2)^2 + (\lambda_2 - \lambda_3)^2 + (\lambda_3 - \lambda_1)^2}}{\sqrt{{\lambda_1}^2 + {\lambda_2}^2 + {\lambda_3}^2}} \quad (10)$$

$$\mathrm{MD} = (\lambda_1 + \lambda_2 + \lambda_3)/3 \quad (11)$$

where λ_i are the eigenvalues of the diffusion tensor associated with the diffusion signal $S(\vec{q})$. There exist two main reasons to justify their choice. First, they are well-understood and standardized in clinical routine. Second, together they contain most of the information that is usually extracted from the dMRI-derived scalar maps [23]. The different region properties (μ_R, Σ_R) measured for the FA and MD joint distribution are summarized in Table I.

IV. Results and Discussion

A. Synthetic gray-scale data

The proposed method solved precisely the specific challenge created by the model. A severe distortion of the model is artificially created adding complexity to the problem of partial voluming in the outer contour of the sulcus. Figure 2 provides visual assessment for this result. With 16x16x16 control points and an approximate total of 29,000 nodes contained by the two prior surfaces, computation time for this model was around 14 minutes in an *Intel® Core™ i5 CPU M 430 @ 2.27GHz* and 4GB RAM.

[1]DTIFIT, included in the FMRIB's Software Library (FSL), http://fsl.fmrib.ox.ac.uk/fsl/fsl-4.1.9/fdt/fdt_dtifit.html

TABLE I
Model means and covariances of FA and MD estimated from the reconstructed simulated dMRI images for each modeled tissue, WM, GM, and CSF. As expected, the two scalar features are complementary and the three tissues can well be discriminated.

	μ	
Tissue	FA	MD
WM	0.778	6.94×10^{-4}
GM	0.119	8.95×10^{-4}
CSF	0.103	2.99×10^{-3}

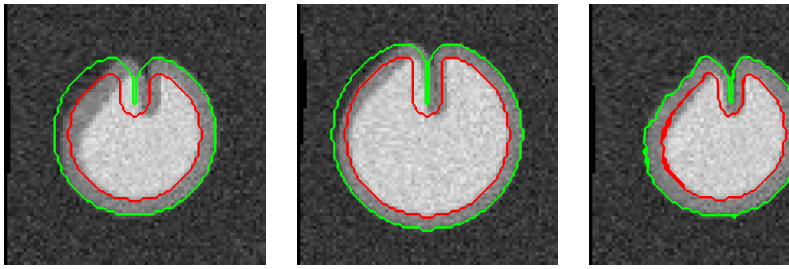

a)

Fig. 2. Result of the segmentation performance on the sulcus model. a) Two slices and prior contours before segmentation-registration. b) The same slices and contours after distortion estimation. c) 3D rendering of the deformed priors, with the traces of the two selected slices highlighted.

B. Simulated diffusion data

The proposed method successfully reverted the synthetic distortion field we applied to the data. Second row in **??** shows the fitted contours obtained by using the original surfaces of the model as shape priors, with a constant translation of [5.0,10.0,-5.0] mm. to illustrate briefly the extent of the capture range of the algorithm. Computation time in this case was around 10 minutes in the previously described platform, with 16x16x16 control points on the dense deformation field and approximately 26,000 nodes in total for both prior surfaces.

V. Conclusion

A novel application for the ACWE framework is proposed, with the aim at recovering the displacement field underlying the EPI geometrical distortions. Exploiting the segmentation properties of the ACWE and optimizing the displacement field, we describe a registration-segmentation methodology

that simultaneously segmented and restored the distortion on dMRI-like synthetic data. Visual results and quantitative results are provided.

We implemented the methodology upon the widely used Insight Registration and Segmentation Toolkit [2] (ITK) for its computational benefits, the standardized code, and with the aim at making the procedure publicly available when ready for sharing with the research community.

Once proven the aptness of the methodology to the application with simplistic synthetic data, in further studies we will cover the actual performance on real images and the benefits of overcoming the described challenges (segmentation and EPI distortion correction) in one single step. Additional research lines regard with the use of more adequate optimization schemes and the use of an energy model better adapted to the specific nature of the dMRI data.

We conclude recalling the importance of tackling with the numerous challenges that exist on the dMRI data processing in order to achieve reliable results on the whole-brain connectivity analysis.

APPENDIX A
PROOF OF DUALITY BETWEEN THE PROBABILISTIC AND THE PRESENTED FRAMEWORKS

Here the demonstration that we are preparing.

In the probabilistic approach to image segmentation, the smoothness constraints can be introduced into the MAP criterium as a Markov Random Field (MRF). Accordingly to the Hammersley-Clifford theorem (**FIXME**: citations needed), an MRF can be equivalently characterized by a Gibb's distribution:

$$P(\mathbf{K}) = \prod_i Z(U)^{-1}\, e^{-U(\mathbf{x}_i|\beta,K)} = const.\, e^{-\sum_i (U(\mathbf{x}_i|\beta,K))} \sim e^{-\nu_B |K|}. \tag{12}$$

This way, we include the assumption that the total length of the edge set K is small and we draw the equivalence with the MRF modeling.

In the probabilistic approach, the underlying concept to segmenting an image is the Bayes' rule. For a discrete image of N pixels indexed by i, this rule reads as follows:

$$P(K|I) = P(I \mid K)\, P(K) = \prod_i p(\mathbf{x}_i|K)\, p_i(K). \tag{13}$$

The normalizer probability $P(I)$ has been ommited for simplicity.

In order to express the likelihood as an absolute energy in our variation framework, the *log*-likelihood is computed:

$$E(K) = -\log(P(K|I)) = \sum_k \int_{\Omega_k} -\log p_k(I(\mathbf{x}),\mathbf{x})\, d\mathbf{x} + \nu_B\, |K|\,, \tag{14}$$

where $\mathbf{s} = I(\mathbf{x})$, $\mathbf{s} \in \mathbb{R}^C$ (a vector of C scalar features). Additionally, the discrete grid of N pixels has been converted to a continuous space by assuming $d\mathbf{x}$ as infinitesimal bin size.

[2] http://www.itk.org

To explicitly define the likelihood, we firstly define the squared *Mahalanobis distance* that is the exponential of a multivariate normal distribution:

$$\Delta_k^2(\mathbf{s}) = (\mathbf{s} - \boldsymbol{\mu}_k)^T\, \Sigma_k^{-1}\, (\mathbf{s} - \boldsymbol{\mu}_k). \tag{15}$$

Therefore, the likelihood is defined as follows:

$$p_k(I(\mathbf{x}),\mathbf{x}) = p_k(\mathbf{s},\mathbf{x}) = p_k(\mathbf{s}) = \frac{1}{\sqrt{(2\pi)^C\ |\boldsymbol{\Sigma}_k|}}\, e^{\left(-\frac{1}{2}\Delta_k^2(\mathbf{s})\right)}. \tag{16}$$

Introducing this definition on (14), we have:

$$E(K) = \sum_k \int_{\Omega_k} -\log\left[\frac{1}{\sqrt{(2\pi)^C\ |\boldsymbol{\Sigma}_k|}}\, e^{\left(-\frac{1}{2}\Delta_k^2(\mathbf{s})\right)}\right] d\mathbf{x} + \nu_B\, |K|\,. \tag{17}$$

$$E(K) = \sum_k \int_{\Omega_k} \left(\frac{1}{2}\log\left((2\pi)^C\ |\boldsymbol{\Sigma}_k|\right) + \frac{1}{2}\Delta_k^2(\mathbf{s})\right) d\mathbf{x} + \nu_B\, |K| \tag{18}$$

$$E(K) = \sum_k \left(\frac{V_k}{2}\log\left((2\pi)^C\ |\boldsymbol{\Sigma}_k|\right) + \frac{1}{2}\int_{\Omega_k} \Delta_k^2(\mathbf{s})\, d\mathbf{x} + \nu_B\, |K|\right) \tag{19}$$

ACKNOWLEDGMENT

The authors gratefully acknowledge V. Estellers for critical discussions at early stages of this project and L. Vese for her generous support.

REFERENCES

[1] P. C. Sundgren, Q. Dong, D. Gómez-Hassan, S. K. Mukherji, P. Maly, and R. Welsh, "Diffusion tensor imaging of the brain: review of clinical applications," *Neuroradiology*, vol. 46, pp. 339–350, May 2004. [Online]. Available: http://www.springerlink.com/content/fa30k4q3h9kg4yjq/

[2] P. Hagmann, "From diffusion MRI to brain connectomics," Ph.D. dissertation, Institut de traitement des signaux PROGRAMME DOCTORAL EN INFORMATIQUE ET COMMUNICATIONS POUR L'OBTENTION DU GRADE DE DOCTEUR ÈS SCIENCES PAR Docteur en médecine, Université de Lausanne, 2005. [Online]. Available: http://biblion.epfl.ch/EPFL/theses/2005/3230/EPFL_TH3230.pdf

[3] O. Sporns, G. Tononi, and R. Kötter, "The human connectome: A structural description of the human brain," *PLoS computational biology*, vol. 1, no. 4, p. e42, Sep. 2005, PMID: 16201007.

[4] A. Daducci, S. Gerhard, A. Griffa, A. Lemkaddem, L. Cammoun, X. Gigandet, R. Meuli, P. Hagmann, and J.-P. Thiran, "The connectome mapper: An open-source processing pipeline to map connectomes with MRI," *PLoS ONE*, vol. 7, no. 12, p. e48121, Dec. 2012. [Online]. Available: http://dx.doi.org/10.1371/journal.pone.0048121

[5] H. Johansen-Berg and M. F. Rushworth, "Using diffusion imaging to study human connectional

anatomy," *Annual Review of Neuroscience*, vol. 32, no. 1, pp. 75–94, 2009, PMID: 19400718. [Online]. Available: http://www.annualreviews.org/doi/abs/10.1146/annurev.neuro.051508.135735

[6] D. K. Jones, T. R. Knösche, and R. Turner, "White matter integrity, fiber count, and other fallacies: The do's and don'ts of diffusion MRI," *NeuroImage*, Jul. 2012, PMID: 22846632.

[7] P. Hagmann, P. E. Grant, and D. A. Fair, "MR connectomics: a conceptual framework for studying the developing brain," *Frontiers in Systems Neuroscience*, vol. 6, Jun. 2012, PMID: 22707934 PMCID: PMC3374479. [Online]. Available: http://www.ncbi.nlm.nih.gov/pmc/articles/PMC3374479/

[8] E. Heiervang, T. Behrens, C. Mackay, M. Robson, and H. Johansen-Berg, "Between session reproducibility and between subject variability of diffusion MR and tractography measures," *NeuroImage*, vol. 33, no. 3, pp. 867–877, Nov. 2006. [Online]. Available: http://www.sciencedirect.com/science/article/pii/S1053811906008081

[9] S. Wakana, A. Caprihan, M. M. Panzenboeck, J. H. Fallon, M. Perry, R. L. Gollub, K. Hua, J. Zhang, H. Jiang, P. Dubey, A. Blitz, P. van Zijl, and S. Mori, "Reproducibility of quantitative tractography methods applied to cerebral white matter," *NeuroImage*, vol. 36, no. 3, pp. 630–644, Jul. 2007. [Online]. Available: http://www.sciencedirect.com/science/article/pii/S1053811907001383

[10] D. Holland, J. M. Kuperman, and A. M. Dale, "Efficient correction of inhomogeneous static magnetic field-induced distortion in echo planar imaging," *NeuroImage*, vol. 50, no. 1, p. 175, Mar. 2010, PMID: 19944768 PMCID: PMC2819607. [Online]. Available: http://www.ncbi.nlm.nih.gov/pmc/articles/PMC2819607/

[11] Y.-C. Hsu, C.-H. Hsu, and W.-Y. Tseng, "Correction for susceptibility-induced distortion in echo-planar imaging using field maps and model-based point spread function," *IEEE Transactions on Medical Imaging*, vol. 28, no. 11, pp. 1850 –1857, Nov. 2009.

[12] P. Jezzard, A. S. Barnett, and C. Pierpaoli, "Characterization of and correction for eddy current artifacts in echo planar diffusion imaging," *Magnetic resonance in medicine*, vol. 39, no. 5, p. 801–812, 2005. [Online]. Available: http://onlinelibrary.wiley.com/doi/10.1002/mrm.1910390518/abstract

[13] P. J. Reber, E. C. Wong, R. B. Buxton, and L. R. Frank, "Correction of off resonance-related distortion in echo-planar imaging using EPI-based field maps," *Magnetic Resonance in Medicine*, vol. 39, no. 2, p. 328–330, 2005. [Online]. Available: http://onlinelibrary.wiley.com/doi/10.1002/mrm.1910390223/abstract

[14] J. L. R. Andersson, C. Hutton, J. Ashburner, R. Turner, and K. Friston, "Modeling geometric deformations in EPI time series," *Neuroimage*, vol. 13, no. 5, p. 903–919, 2001. [Online]. Available: http://www.sciencedirect.com/science/article/pii/S1053811901907463

[15] L. Zöllei, A. Stevens, K. Huber, S. Kakunoori, and B. Fischl, "Improved tractography alignment using combined volumetric and surface registration," *NeuroImage*, vol. 51, no. 1, pp. 206–213, May 2010. [Online]. Available: http://www.sciencedirect.com/science/article/pii/S1053811910001400

[16] T. F. Chan and L. A. Vese, "Active contours without edges," *IEEE Transactions on Image Processing*, vol. 10, no. 2, p. 266–277, 2001.

[17] M. Bertero, T. A. Poggio, and V. Torre, "Ill-posed problems in early vision," in *Proceedings of the IEEE*, vol. 76, 1988, p. 869–889.

[18] J. Hadamard, "Sur les problèmes aux dérivées partielles et leur signification physique," *Princeton University Bulletin*, vol. 13, p. 49–52, 1902.

[19] V. A. Morozov, "Linear and nonlinear ill-posed problems," *Journal of Mathematical Sciences*, vol. II, no. 6, p. 706–736, 1975.

[20] A. N. Tichonov, "Solution of incorrectly formulated problems and the regularization method," *Soviet Mathematics*, vol. 4, p. 1035–1038, 1963.

[21] H.-H. Nagel and W. Enkelmann, "An investigation of smoothness constraints for the estimation of displacement vector fields from image sequences," *IEEE Transactions on Pattern Analysis and Machine Intelligence*, vol. PAMI-8, no. 5, p. 565–593, Sep. 1986. [Online]. Available: http://ieeexplore.ieee.org/lpdocs/epic03/wrapper.htm?arnumber=4767833

[22] D. MacDonald, N. Kabani, D. Avis, and A. C. Evans, "Automated 3-d extraction of inner and outer surfaces of cerebral cortex from MRI," *NeuroImage*, vol. 12, no. 3, p. 340, 2000. [Online]. Available: http://citeseerx.ist.psu.edu/viewdoc/download?doi=10.1.1.73.8698&rep=rep1&type=pdf

[23] D. B. Ennis and G. Kindlmann, "Orthogonal tensor invariants and the analysis of diffusion tensor magnetic resonance images," *Magnetic Resonance in Medicine*, vol. 55, no. 1, p. 136–146, 2006. [Online]. Available: http://onlinelibrary.wiley.com/doi/10.1002/mrm.20741/abstract

PLACE PHOTO HERE

Oscar Esteban Biography text here.